

An upper limit for water dimer absorption in the 750 nm spectral region and a revised water line list

A. J. L. Shillings¹, S. M. Ball², M. J. Barber³, J. Tennyson³, and R. L. Jones¹

¹Department of Chemistry, University of Cambridge, Cambridge, CB2 1EW, UK

²Department of Chemistry, University of Leicester, Leicester, LE1 7RH, UK

³Department of Physics and Astronomy, University College London, London, WC1E 6BT, UK

Received: 2 August 2010 – Published in Atmos. Chem. Phys. Discuss.: 11 October 2010

Revised: 19 April 2011 – Accepted: 23 April 2011 – Published: 9 May 2011

Abstract. Absorption of solar radiation by water dimer molecules in the Earth's atmosphere has the potential to act as a positive feedback effect for climate change. There seems little doubt from the results of previous laboratory and theoretical studies that significant concentrations of the water dimer should be present in the atmosphere, yet attempts to detect water dimer absorption signatures in atmospheric field studies have so far yielded inconclusive results. Here we report spectral measurements in the near-infrared around 750 nm in the expected region of the $|0\rangle_f |4\rangle_b |0\rangle$ overtone of the water dimer's hydrogen-bonded OH stretching vibration. The results were obtained using broadband cavity ringdown spectroscopy (BBCRDS), a methodology that allows absorption measurements to be made under controlled laboratory conditions but over absorption path lengths representative of atmospheric conditions. In order to account correctly and completely for the overlapping absorption of monomer molecules in the same spectral region, we have also constructed a new list of spectral data (UCL08) for the water monomer in the 750–20 000 cm^{-1} (13 μm –500 nm) range.

Our results show that the additional lines included in the UCL08 spectral database provide an improved representation of the measured water monomer absorption in the 750 nm region. No absorption features other than those attributable to the water monomer were detected in BBCRDS experiments performed on water vapour samples containing dimer concentrations up to an order of magnitude greater than expected in the ambient atmosphere. The absence of detectable water dimer features leads us to conclude that, in the absence of significant errors in calculated dimer oscillator strengths or monomer/dimer equilibrium constants, the widths of any

water dimer absorption features present around 750 nm are of the order of 100 cm^{-1} HWHM, and certainly greater than the 25–30 cm^{-1} HWHM reported in the literature for lower energy water dimer transitions up to 8000 cm^{-1} .

1 Introduction

Absorption of solar radiation by water dimers in the Earth's atmosphere has potentially important consequences for the planet's radiative balance and for amplifying the feedback effects of climate change (e.g. Chýlek and Geldart, 1997). Much of the early laboratory work investigating the spectroscopy of water dimers was performed under the non-equilibrium conditions of molecular beams (Odotola and Dyke, 1980; Huisken et al., 1996; Paul et al., 1997, 1998; Nizkorodov et al., 2005) or, more recently, on dimers formed at very low temperatures inside rare gas matrixes (Bouteiller and Perchard, 2004) and helium nano-droplets (Kuyanov-Prozument et al., 2010). Although offering many insights into the fundamental properties of water dimers (e.g. Fellers et al., 1999), such methods cannot provide direct measurements of water dimer absorptions under “normal” atmospheric conditions (ambient temperatures and pressures, and for typical water monomer amounts). Instead, there have been several attempts to detect signs of water dimer absorption directly in atmospheric field studies, with authors variously reporting a dimer absorption band around 750 nm (Pfeilsticker et al., 2003), a potential weak but inconclusive dimer signal in the same region (Sierk et al., 2004) or no observable dimer absorptions at all (Daniel et al., 1999; Hill and Jones, 2000). This disparity in field results has prompted further laboratory investigations into the absorption properties of the water dimer and/or water continuum



Correspondence to: R. L. Jones
(rlj1001@cam.ac.uk)

under atmospherically relevant conditions. These studies have tended to concentrated on infrared frequencies up to 8000 cm^{-1} , including the fundamental, first overtone and first combination band vibrations of the water monomer. In these regions, absorption features consistent with those expected for the water dimer have been observed underlying the monomer bands (e.g. Ptashnik et al., 2004, 2011; Paynter et al., 2007, 2009; Ptashnik, 2008) at frequencies that are broadly consistent with theoretical predictions of the dimer's spectrum (Low and Kjaergaard, 1999; Schofield and Kjaergaard, 2003; Schofield et al., 2007; Garden et al., 2008). Additional laboratory studies at frequencies in between water monomer lines report results that are broadly consistent with models of the water continuum absorption (Aldener et al., 2005; Cormier et al., 2005). But at higher frequencies, a laboratory study by Kassi et al. (2005) was unable to reproduce an absorption feature seen near 750 nm in field observations by the Pfeilsticker et al. (2003) and initially attributed to the water dimer (although this claim to have observed the water dimer has since been revoked, Lotter, 2006).

Here we report results of a broadband cavity ringdown spectroscopy study performed to attempt to detect the third overtone of water dimer's hydrogen-bonded OH_b stretching vibration which the theoretical studies predict to occur around 750 nm with an oscillator strength similar to the monomer itself. As noted previously by Kassi et al. (2005), one very important aspect of spectroscopic studies of the water dimer is the need to account correctly and completely for overlapping absorption of monomer molecules in the same spectral region. For this purpose, and particularly because we probe spectra above room temperature where standard databases can be expected to be less reliable, we have also constructed and tested a new list of spectral data for the water monomer which is reported below.

1.1 Water dimer abundance

Water dimers form in the atmosphere from the (reversible) association of two water molecules.



Consequently the concentration of water dimers depends on the square of the water monomer concentration and the equilibrium constant, K_{eq} , for dimer formation:

$$K_{\text{eq}} = [(\text{H}_2\text{O})_2]/[\text{H}_2\text{O}]^2 \quad (1b)$$

and thus $[(\text{H}_2\text{O})_2] = K_{\text{eq}} [\text{H}_2\text{O}]^2$

Dimer concentrations in the atmosphere will vary with temperature due to a combination of the equilibrium constant's dependence on temperature, and because the water monomer's saturated vapour pressure increases approximately exponentially with temperature. The literature contains a number of estimates of the equilibrium constant for

dimer formation derived from both experimental and theoretical approaches. Curtiss et al. (1979) measured the thermal conductivity of steam over a range of temperatures and pressures, and then inferred K_{eq} and ΔH (and so too ΔS) for the dimer formation process. Harvey and Lemmon (2004) inferred K_{eq} from second virial coefficient (B) data derived from vaporisation measurements using the relationship $K_{\text{eq}}(T) = -(B-b_0)/RT$ where b_0 is the excluded volume. Paynter et al. (2007) estimated K_{eq} by fitting water dimer absorption features (from the theoretical study of Schofield and Kjaergaard, 2003) to residuals remaining after fitting the monomer absorption in water vapour spectra between 3100 and 4400 cm^{-1} .

The equilibrium constant can also be calculated from the molecular partition functions for the monomer and dimer and the dimer's dissociation energy (Vigasin, 2000). The calculation relies on an accurate potential surface being available from which the dimer's energy levels and hence partition function are found. This theoretical approach is made complicated because some uncertainty exists as to which states should be included when calculating the dimer partition function (Ptashnik et al., 2011), in part because the dissociation energy is not sufficiently well constrained. For example, Scribano et al. (2006) showed that an error of 4% (50 cm^{-1}) in the dissociation energy (1234 cm^{-1} , 15 kJ mol^{-1}) could lead to an error of 26% in the calculated dimer equilibrium constant.

Estimates of K_{eq} from the experimental studies described above and from the theoretical studies of Munoz-Caro and Nino (1997), Goldman et al. (2004) and a further refinement using fewer approximations by the latter group (Scribano et al., 2006) are summarised in the upper panel of Fig. 1. The points represent K_{eq} values reported in the literature, the solid line comes from the study of Scribano et al. (2006) which explicitly addresses the temperature dependence of K_{eq} , and the broken lines were calculated using data given by their original authors assuming that ΔH and ΔS for dimer formation are independent of temperature (an assumption that Scribano et al. (2006) showed is not strictly valid). The main feature of the plot is that K_{eq} decreases as temperature increases, which is characteristic of a weakly bound molecular complex. There are also significant differences in the various K_{eq} determinations, particularly for the lower temperatures shown on the graph which correspond to those encountered in the atmosphere.

Using the median K_{eq} estimate from Curtiss et al. (1979) for a typical mid-latitude atmospheric temperature (25°C) and water vapour concentration ($4 \times 10^{17}\text{ molecules cm}^{-3} \approx 1.6\%$ mixing ratio), the calculated water dimer concentration is $2.4 \times 10^{14}\text{ molecules cm}^{-3}$ i.e. 0.06% of the monomer concentration. This low value partly explains why there have been relatively few studies of water dimer absorption under atmospheric conditions and why laboratory studies of water dimers have often used the non-equilibrium conditions of molecular beams where

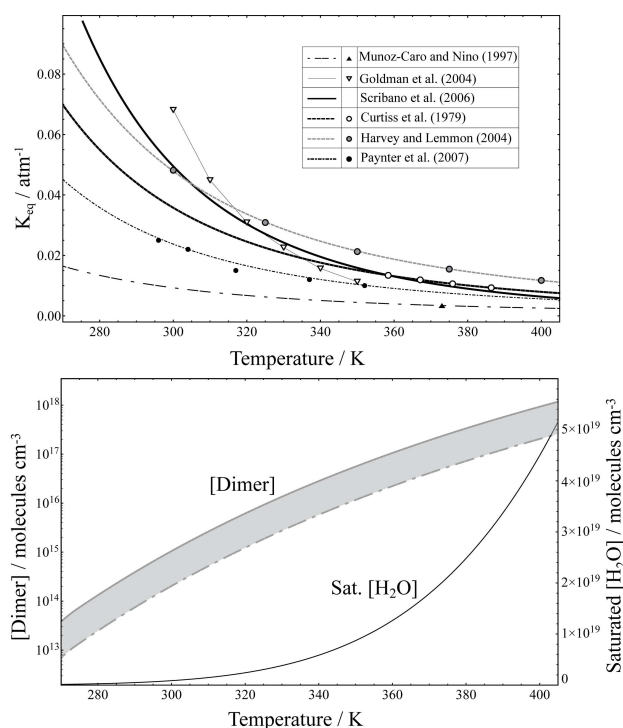


Fig. 1. Upper panel: Temperature dependence of the equilibrium constant for formation of the water dimer. Lower panel: number concentration of water monomer at saturation as a function of temperature (black line; right axis), and corresponding number concentration of the dimer (shaded area; left axis) calculated using the various equilibrium constants above for an assumed relative humidity of 85 %.

conditions can be adjusted to maximise the mole fraction of the dimer present.

The shaded area of the lower panel of Fig. 1 shows the range of predicted water dimer concentrations as a function of temperature (assuming a relative humidity of 85 %, i.e. conditions readily achievable in a laboratory study) for the range of K_{eq} determinations in the figure's upper panel. Although K_{eq} decreases with increasing temperature, dimer concentrations increase rapidly at higher temperatures due to the $[\text{H}_2\text{O}]^2$ term in Eq. (1b). This also implies that the climate feedback effect of water dimer absorption is likely to be positive.

1.2 Theoretical studies of the water dimer absorption

The vibrational modes of the donor unit of the water dimer are labelled by $|x\rangle_f |y\rangle_b |z\rangle$ where x is the number of vibrational quanta in the unbound “free” OH_f mode, y is the number of quanta in the OH_b mode (where the H_b atom forms the hydrogen bond with the acceptor unit) and z is the number of bending quanta (Schofield and Kjaergaard, 2003). In the acceptor unit, where the two OH bonds are identical, the notation used is $|xy\rangle_{+-} |z\rangle$, with x , y and z having the

same meaning as before. The transition of interest for the current work is $|0\rangle_f |4\rangle_b |0\rangle$, i.e. the transition from the vibrational ground state exciting 4 quanta in the OH_b vibration. As discussed by Pfeilsticker et al. (2003) and Schofield and Kjaergaard (2003), transitions of this type are particularly promising for detecting water dimer absorption signatures as the OH_b bond has been weakened by the act of hydrogen bonding and so transitions exciting this bond are red-shifted. Indeed, the predicted red-shifting is such that these dimer transitions occur at the edges of or even in between the main monomer bands where, because the monomer absorption is much weaker, any dimer transitions ought to be more readily identifiable. Thus the spectral region selected for this work (the shaded area in Fig. 2) was chosen to span the positions of the red-shifted $|0\rangle_f |4\rangle_b |0\rangle$ absorption features predicted from theory. The water dimer bands plotted in the lower panel of Fig. 2 have been selected to illustrate the range of band positions and intensities resulting from the different theoretical approaches (Low and Kjaergaard, 1999; Schofield and Kjaergaard, 2003; Schofield et al., 2007). For comparison, the upper panel of Fig. 2 shows high resolution water monomer cross sections calculated using our UCL08 line list.

To generate the dimer absorption spectra in Fig. 2 we followed the convention of Schofield and Kjaergaard (2003) who assumed a Lorentzian line shape. We have assumed a line width of 25 cm^{-1} half width at half maximum (HWHM) which is representative of the various experimentally observed features assigned to the water dimer by previous investigators. The features observed by Ptashnik et al. (2004) around 5300 cm^{-1} had a HWHM of either 18 cm^{-1} or 28 cm^{-1} depending upon which model of the water vapour continuum absorption was used in the retrievals, and those from Paynter et al. (2007) around 3700 cm^{-1} also had a HWHM of 28 cm^{-1} . Ptashnik et al. (2011) have recently reviewed the various experimental observations of the water self-continuum in the near-infrared, and conclude that the full widths at half maximum of individual water dimer bands are $50\text{--}60 \text{ cm}^{-1}$ FWHM (i.e. $25\text{--}30 \text{ cm}^{-1}$ HWHM). The OH-stretching overtones in gas phase spectra of other molecules such as phenol (Ishichi et al., 2006) have also been observed with bandwidths around 20 cm^{-1} HWHM. In their theoretical paper, Schofield and Kjaergaard (2003) suggest a HWHM of 20 cm^{-1} for water dimer transitions.

2 Broadband cavity ringdown spectroscopy

Broadband cavity ringdown spectroscopy (BBCRDS) uses light from a pulsed broadband laser to measure the spectrum of weakly absorbing samples contained within a high finesse optical cavity (Ball and Jones, 2003, 2009). A multivariate fit of reference absorption cross sections to structured features in the sample's absorption spectrum is then performed

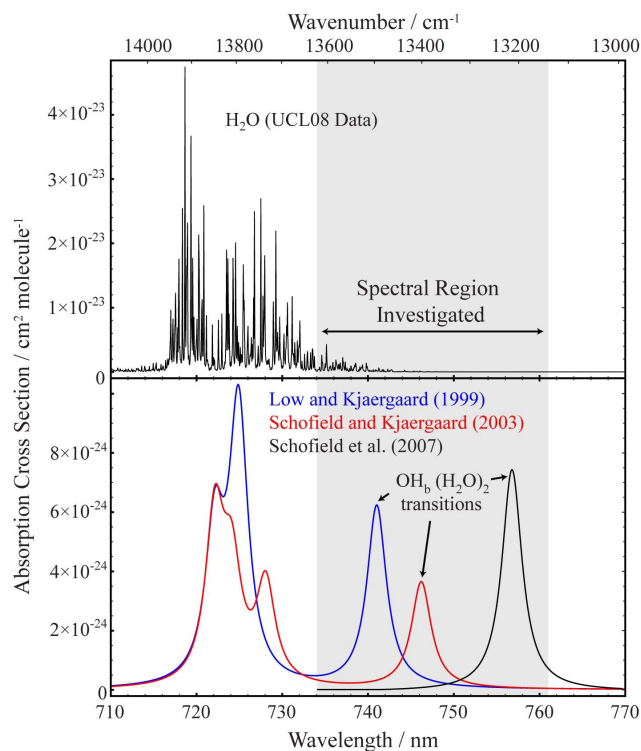


Fig. 2. Water dimer absorption bands for the $|0\rangle_f |4\rangle_b |0\rangle$ OH_b stretching overtone (and nearby dimer transitions) predicted by theoretical studies (lower panel). The dimer bands are shown for an assumed Lorentzian line profile of 25 cm^{-1} HWHM. The upper panel shows high resolution absorption cross sections of the water monomer calculated with the UCL08 line list (air broadened lines). The shaded region indicates the wavelength range of the BCRDS measurements.

using an analysis similar to that developed for differential optical absorption spectroscopy (DOAS) (Platt, 1999) in order to identify the species that make structured contributions to the total measured absorption. For our application, the BCRDS approach has significant advantages over DOAS. Firstly, since it is possible to record an accurate background spectrum (recorded in the absence of absorbing species), an absolute rather than differential absorption spectrum can be obtained. Consequently it is possible to identify and separately quantify not only structured absorbers present in the total measured signal (i.e. water monomer) but also relatively unstructured absorbers whose features vary only slowly with wavelength and may extend over a large spectral range (i.e. water dimer). Secondly, conventional DOAS requires the use of very long paths to achieve the sensitivity necessary to investigate weak absorption signals. Such paths can only be realised in the real atmosphere where experimental conditions (temperature and $[\text{H}_2\text{O}]$) cannot be controlled and are potentially inhomogeneous over the light path. In BCRDS, the very long effective pathlengths (up to 60 km in this work) are achieved within an absorption cell, defined by a high finesse

cavity that is only some 2 m in length, thus enabling experimental conditions to be tightly and reproducibly controlled.

A broadband dye laser pumped by a 532 nm Nd:YAG laser (Sirah Cobra & Surelight I-20) generated light pulses (10 ns, 20 Hz repetition rate) with an approximately Gaussian emission spectrum centred at 748 nm (FWHM = 16.5 nm). This light was directed into a 196 cm long ringdown cavity formed by two highly reflective mirrors (Los Gatos, measured peak reflectivity = 99.994 % at 765 nm). Light exiting the ringdown cavity was collected and conveyed through a 200 μm core diameter fibre optic cable to an imaging spectrograph (Chromex 250is) where it was dispersed in wavelength and imaged onto a clocked CCD camera (XCam CCDRem2). The time evolution of individual ringdown events was recorded simultaneously at 512 different wavelengths, one for each pixel row of the detector, and light from 50 ringdown events was integrated on the CCD camera before storing the data to a computer. Wavelength resolved ringdown times were produced by fitting the ringdown decay in each pixel row. The sample's absorption spectrum was then calculated from sets of ringdown times measured when the cavity contained the sample, $\tau(\lambda)$, and when flushed with dry synthetic air, $\tau_0(\lambda)$:

$$\alpha(\lambda) = \frac{R_L}{c} \left(\frac{1}{\tau(\lambda)} - \frac{1}{\tau_0(\lambda)} \right) = \alpha_{\text{cont}}(\lambda) + \sum_n \alpha_n(\lambda) \quad (2)$$

Here c is the speed of light, R_L is the ratio of the total cavity length to the length of the cavity that is occupied by the absorbing gas sample, $\alpha_n(\lambda)$ is the wavelength dependent absorption coefficient of the n^{th} molecular absorber and $\alpha_{\text{cont}}(\lambda)$ is any remaining unstructured continuum absorption.

A known complexity that must be accounted for in the analysis of BCRDS spectra is the apparent non-Ber-Lambert law behaviour exhibited by strong absorption lines that are not fully resolved at the limited resolution of the instrument's spectrograph (here 0.22 nm FWHM). As discussed in detail in Ball and Jones (2003), Bitter et al. (2005) and Ball and Jones (2009), this effect is treated quantitatively using linearised absorption cross sections, and this approach was adopted here for generating reference cross sections for the water monomer. The linearised absorption cross sections were produced as follows. High resolution absorption cross sections of the water monomer (appropriate to the temperature of each experiment) were generated from a line-by-line calculation using line positions and intensities, ground state energies and air- and self-broadening coefficients from the new UCL08 line list (Voigt line shapes; 0.0005 nm wavelength grid). These cross sections were used to calculate high resolution transmission spectra though representative column amounts of water vapour traversed by the light whilst confined inside the ringdown cavity. Typically 350 such transmission spectra were generated, spanning the time evolution of the ringdown event as recorded on

the clocked CCD camera. A hygrometer (Vaisala HMT 330) provided a measurement of the water vapour concentration inside the ringdown cavity to inform the relative amounts of air- and self-broadening used in calculating the high resolution cross sections, and the range of water columns needed to calculate the various high resolution transmission spectra. The high resolution transmission spectra were then degraded to the instrument resolution by convolving them with the instrument function (measured using essentially monochromatic lines from a neon atomic emission lamp). The resulting low resolution transmission spectra were converted to spectra of optical depth, and the optical depth at the central wavelength of each pixel of the CCD camera was plotted as a function of water column amount. For pixels viewing wavelengths where the sample remains optically thin for all column amounts sampled during the ringdown event, the plot is a straight line with a gradient equal to the absorption cross section of the water monomer at the spectral resolution of the BCCRDS spectrometer. However, the plot of optical depth versus column amount is curved for pixels sampling wavelengths that include strong absorption lines that saturate at the large water column amounts probed during the ringdown event. But crucially the curvature of the plot is the same as the curvature of the (natural logarithm of the) ringdown signal versus time, and thus a linearised cross section derived from a linear regression of the column-dependent optical depth represents the average cross section (at the spectrometer's resolution) presented by water molecules during the multi-exponential ringdown decay. Linearised cross sections were generated in the same way starting from the HITRAN08 dataset in order to test fitting the BCCRDS spectra with this line list too.

Measurements were made on continuously flowing gas samples supplied to the ringdown cavity via flow controllers, a temperature regulated water bubbler and particle filters. The temperature inside the cavity was controlled by circulating heated/cooled water from a thermostated water bath through an insulated, double-walled glass vessel enclosing the length of the cavity. Gas delivery lines were constructed to prevent cold spots and passed between the glass vessel and its insulation in order to prevent condensation and to enable the gas supply to be admitted at the same temperature as the cavity itself. Temperatures between 5 and 95 °C and relative humidities up to 95 % were achieved with no aerosol formation and negligible temperature gradients along the cavity. The gas flow exited past the cavity mirrors and was vented into the laboratory: thus all experiments were performed under ambient pressure with the sample occupying the whole cavity ($R_L = 1$ in Eq. 2). To prevent condensation of water vapour on the surface of the cavity mirrors (which would have reduced their reflectivity and produced an anomalous absorption signal), the mirrors were held in temperature controlled mirror mounts regulated at approximately 3 °C above the cavity's temperature. This approach was found both to eliminate condensation on the mirror surfaces and, some-

what unexpectedly, to improve the reflectivity of the mirrors by approximately 10 % relative to that at room temperature, presumably due to desorption of adsorbed species from the hot mirror surfaces.

3 The UCL08 line list

The HITRAN 2008 database (Rothman et al., 2009) provides a good quality reference for water's strong absorption lines in most spectral regions. However, having a relatively high cut-off in line strength intensity, it omits many weak lines which are known to be present from *ab initio* calculations and which can become important in long path length absorption experiments such as those reported here. The present line list, which we name UCL08, therefore attempts to fill in such gaps as there are in the HITRAN database using a combination of new experimental data and, in the absence of measurements, theoretical lines from the calculated BT2 linelist (Barber et al., 2006). To improve the accuracy of the calculated transition frequencies, a version of BT2 modified to use experimental energy levels from Tennyson et al. (2001) rather than purely theoretical ones was used.

The UCL08 line list covers the 750–20 000 cm^{-1} spectral range at the default HITRAN temperature of 296 K. The list was compiled as part of the "Continuum Absorption at Visible and Infrared Wavelengths and its Atmospheric Relevance" (CAVIAR) consortium project which involves a series of laboratory experiments, atmospheric observations and climate modelling calculations. The 750–20 000 cm^{-1} range covers most CAVIAR activities, except for some far-infrared work where the cut-off levels for HITRAN lines are much smaller and HITRAN was considered to be sufficient.

The UCL08 line list was constructed as follows. Lines from new experimental sources (Jenouvrier et al., 2007; Mikhailenko et al., 2007, 2008; Coudert et al., 2008; Tolchenov and Tennyson 2008) were taken as first preference. There was no need for any ranking within these experimental sources since none of them include overlapping entries. Lines from HITRAN08 were then used in preference to theoretical data where both transitions were present. Finally, BT2 was used for lines not listed in either the new experimental sources or HITRAN. The exception was the 8000–9500 cm^{-1} spectral region where intensities from BT2 were preferred because of an apparent systematic error in HITRAN08 for this region (see below). To avoid duplication, lines were matched between the different sources based upon their quantum numbers. Since not all BT2 lines are assigned with a full set of rotational and vibrational quantum numbers, we instead used the parity of the upper and lower states in this case, which can be derived from the rotational and vibrational numbers. The few remaining unmatched lines were checked manually for lines of similar frequency and intensity. Despite this, there remains a possibility of duplicated lines where assignments are radically different. However,

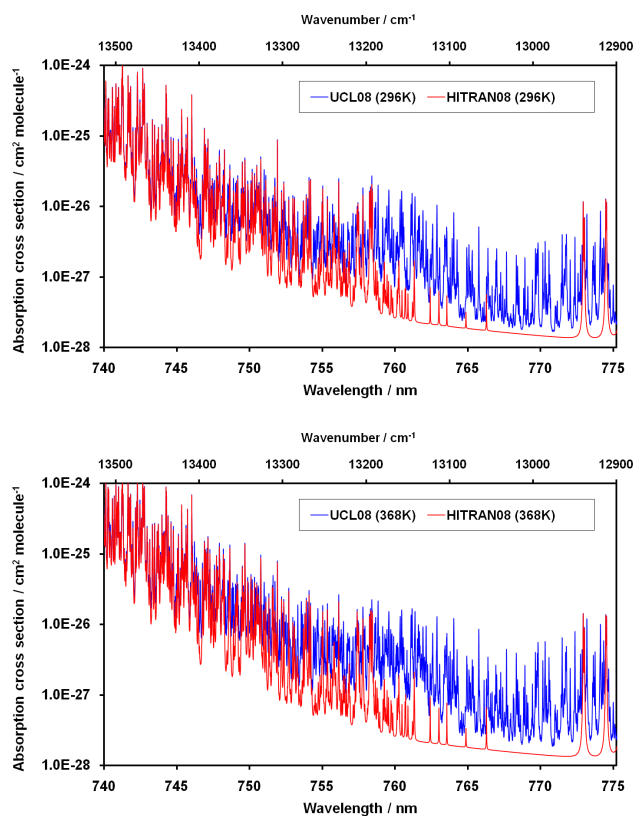


Fig. 3. Comparisons of water monomer absorption cross sections on the low frequency side of the 720 nm water band in the region of the dimer's red-shifted $|0\rangle_f |4\rangle_b |0\rangle$ OH_b stretching overtone. Cross sections from the HITRAN08 (Rothman et al., 2009; red) and UCL08 line lists (this work; blue) are shown for 296 K and 386 K in the upper and lower panels respectively.

these will generally be weak lines and some of these will be offset by corresponding mismatches.

Line broadening parameters in UCL08 are taken from HITRAN where available. Otherwise line widths for non-HITRAN lines were estimated using a method based on fitting to lines with similar quantum numbers (Voronin et al., 2010). This method has been demonstrated to provide a reasonable fit to known widths given in HITRAN. All isotopologues are taken from HITRAN. Ideally, we would have liked to use a theoretical database similar to BT2 to fill these, although most of the missing lines will be rather weak ones. Since the line list was initially prepared in 2008, some later experimental papers have been published containing relevant results not currently included in UCL08. Should a future need arise, it would be relatively easy to incorporate them, however.

Figure 3 shows a comparison of high resolution water monomer cross sections calculated from the HITRAN08 and UCL08 line lists in the region expected for the $|0\rangle_f |4\rangle_b |0\rangle$ dimer absorption, and illustrates the large number of additional lines at the edge of the water monomer band present

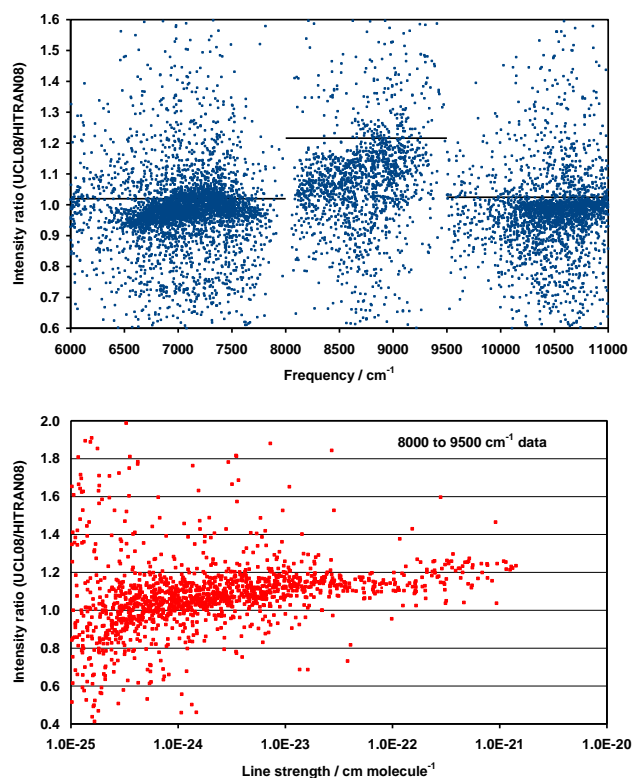


Fig. 4. Upper panel: The ratio of line strengths for water monomer lines common to the HITRAN08 and UCL08 lists. The heavy horizontal lines indicate the intensity-weighted average of the line strength ratios in the spectral regions 6000–8000 cm⁻¹ (average = 1.0198), 8000–9500 cm⁻¹ (1.216) and 9500–11 000 cm⁻¹ (1.025). Lower panel: ratio of UCL08/HITRAN08 intensities as a function of line strength for lines between 8000 and 9500 cm⁻¹. The strong lines, which necessarily dominate the intensity-weighted average, typically have ratios around 1.2. The majority of the weaker lines also show intensity ratios between 1.0 and 1.2, suggesting the difference is systematic.

in the new line list. Note also that these extra lines tend to increase in intensity at the elevated temperatures used in the BCRDS experiments, as demonstrated in the lower panel of Fig. 3 which shows a comparison of HITRAN08 and UCL08 monomer cross sections calculated for 386 K.

The upper panel of Fig. 4 shows the ratios of intensities for lines common to the UCL08 and HITRAN08 databases for three near-infrared water monomer absorption bands. The UCL08 and HITRAN08 averaged line strengths typically agree to within 2.5 % (which is within the uncertainty of the new database), as is the case for two of the three bands shown in Fig. 4. However, there is a systematic intensity-weighted average difference of around 20 % in the 8000–9500 cm⁻¹ region, the HITRAN lines being weaker than those in the UCL08 database (see also the lower panel of Fig. 4). Additional support for our use of the theoretical intensities from the BT2 linelist as first preference for UCL08

in the 8000–9500 cm^{-1} region is provided by Casanova et al. (2006) who compared high resolution Fourier transform measurements of solar radiation at ground level with that modelled using HITRAN04 water vapour lines: whilst there was good agreement in other spectra regions, the modelled absorption underestimated the measured absorption by 18 % between 8000 and 9500 cm^{-1} (a discrepancy similar to the average intensity ratio shown in Fig. 4).

There are two versions of the new UCL08 line list. One contains around two hundred thousand lines with a line intensity cut-off at $S = 10^{-30}$ cm molecule^{-1} , whereas the longer version has around 1.5 million lines with a 10^{-36} cm molecule^{-1} cut-off. The short list should be sufficient for comparison with experimental results in most spectral regions. The long list should provide a good model for water vapour spectra up to about 300 °C, and for high temperatures use of BT2 directly is recommended. Both new line lists are presented in the supplementary data for this article, together with a file of temperature-dependent line strengths (296–368 K) for the nearly sixty thousand lines from the short list in the frequency range 12 750–20 000 cm^{-1} .

4 Results

4.1 BBRDS measurements in the 750 nm spectral region

As noted above, when searching for water dimer absorption signals, it is vital to account fully for water monomer lines in measured spectra, including weak lines at the edge of the monomer's absorption bands some of which may be incorrectly parameterised in (or indeed missing from) the spectral databases. In order to test the efficacy of our new UCL08 line list relative to HITRAN08 in the region expected for the dimer's $|0\rangle_f |4\rangle_b |0\rangle$ overtone, BBRDS spectra of water vapour were recorded in synthetic air at atmospheric pressure for a variety of water monomer concentrations and temperatures. As an example, the top panel of Fig. 5 shows a BBRDS spectrum of water vapour obtained at 312 K with a water concentration of 1.41×10^{18} molecules cm^{-3} (approx. 85 % relative humidity at 312 K). The elevated temperature is used here (i) to increase the water monomer concentration above that at room temperature in order to also increase the intensity of weak water monomer lines and (ii) to test the water databases under the experimental conditions that will be used in the following sections to maximise the water dimer concentration in the gas sample during experiments targeting the dimer (c.f. the discussion in Sect. 1.1). The red line overlaying the blue BBRDS spectrum is the fitted water monomer absorption calculated using linearised absorption cross sections at the BBRDS spectrometer's resolution, constructed using the HITRAN08 line list. The HITRAN spectrum accounts reasonably well for the water monomer lines, yet small systematic differences remain in the residual

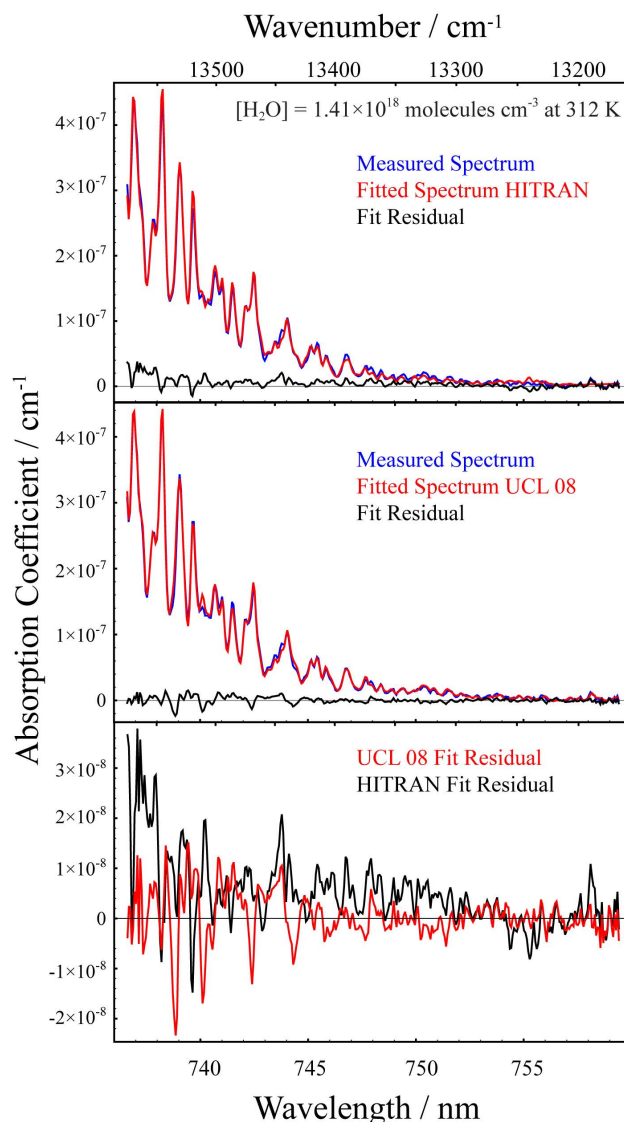


Fig. 5. BBRDS spectrum of water vapour at approx 85 % RH and 312 K recorded in air at 1 atmosphere total pressure. The BBRDS spectrum (blue) is fitted with monomer absorption cross sections calculated using the HITRAN08 (red, top panel) and UCL08 line lists (red, middle panel). The residual spectra are shown in black, and are reproduced on an expanded scale in the bottom panel.

spectrum (measured minus fitted; black line). The middle panel of Fig. 5 shows the same BBRDS spectrum (blue), but this time fitted with linearised absorption cross sections calculated using the UCL08 line list (red). Some small features again remain in the residual spectrum (black).

The bottom panel of Fig. 5 shows the residuals from the upper two panels plotted on an expanded vertical scale. Although neither spectral database provides a comprehensive description of the water monomer lines, the standard deviation of the UCL08 residual (5.31×10^{-9} cm^{-1}) is somewhat smaller than for HITRAN08 (5.75×10^{-9} cm^{-1}). The

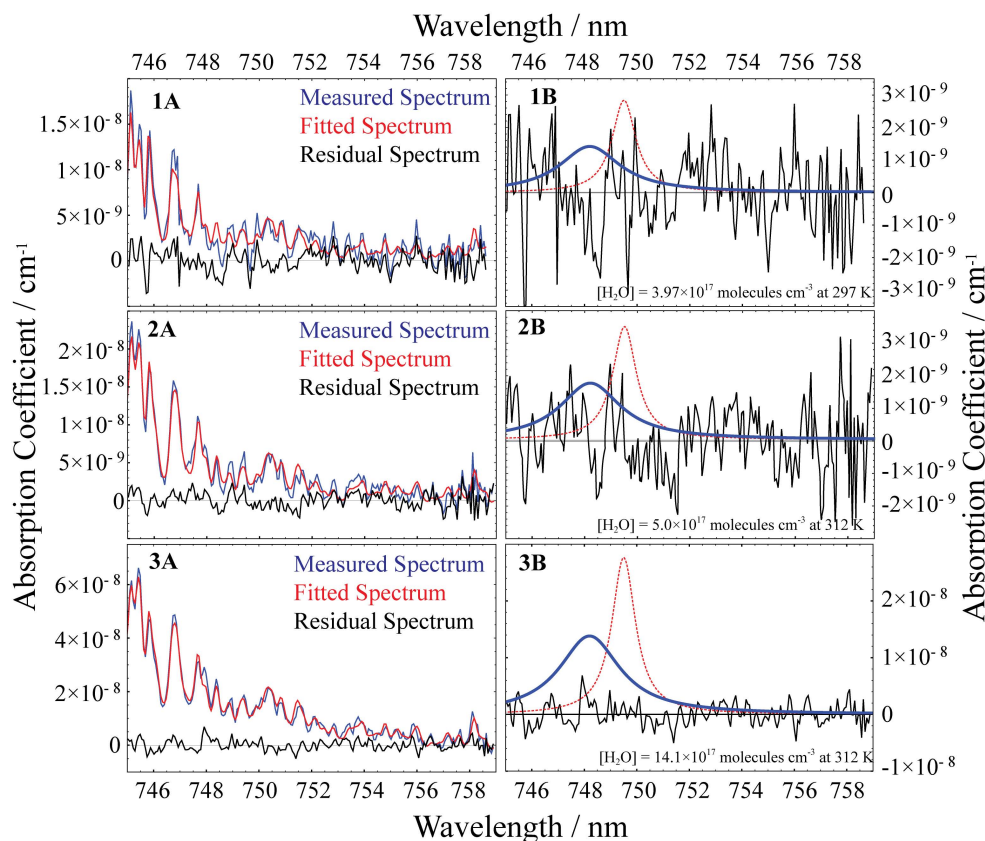


Fig. 6. Panels 1A, 2A and 3A: BBRDS spectra (blue), corresponding fitted monomer absorption spectra (red; UCL08 line list) and residuals (measurement minus fit; black) for water monomer concentrations of 3.97×10^{17} molecules cm^{-3} at 297 K, 5.0×10^{17} molecules cm^{-3} at 312 K, and 1.41×10^{18} molecules cm^{-3} at 312 K. Panels 1B, 2B and 3B show the residual spectra again (black), overlaid by a Lorentzian function (blue) representing a generic dimer OH_b stretching band having the average line position and band intensity of the theoretical predictions shown previously in Fig. 2 (748.2 nm, $S = 4.5 \times 10^{-22}$ cm molecule $^{-1}$, 25 cm^{-1} HWHM). This dimer band has been assumed to scale with the square of the water monomer concentration and to scale with temperature according to the Curtiss et al. (1979) equilibrium constant. The dotted red line shows a Lorentzian function with the centre wavelength, width and intensity of the absorption feature in Pfeilsticker et al. (2003), again scaled according to $[\text{H}_2\text{O}]^2$ and the $K_{\text{eq}}(T)$ of Curtiss et al. (1979). See text for further details.

UCL08 line list generally provides a better fit to the strong water lines on the edge the monomer band at short wavelength; it also has smaller residuals at wavelengths longer than 745 nm where, there being only weak monomer absorption, the UCL08 residual is mainly due to measurement noise. In contrast, the HITRAN08 residual shows a broad positive feature in the region 745–752 nm, similar in some respects to a dimer absorption feature. However we discount this as a possible dimer feature because it scales approximately linearly (rather than quadratically) with water monomer concentration and because it is not reproduced using the UCL08 line list that provides the better fit to the water monomer structure in this spectral region. Instead this feature is probably a consequence of weak monomer lines missing from HITRAN08 but included in the UCL08 list; other studies of the water monomer's spectroscopy in this region (Kassi et al., 2005; Campargue et al., 2008) have found many more weak absorption lines than are included in the HITRAN line

list (see Sect. 4.2 below). In contrast, no dimer-like absorption features are immediately obvious in the UCL08 residual.

4.2 Comparison with dimer absorption features

Figure 6 shows absorption spectra recorded at 297 and 312 K for water vapour diluted in synthetic air ($P_{\text{total}} = 1$ atm). Panels 1A, 2A and 3A focus on the long-wavelength part of the BBRDS bandwidth, right on the edge of the water monomer band where a red-shifted OH stretching overtone of the dimer would be most readily observable. The new UCL08 database, which was shown in the previous section to provide the best representation of the water monomer structure in this spectral region, was used exclusively for the analysis of BBRDS spectra presented in this section and the remainder of this paper. The water vapour concentration and temperature for the spectrum in Panel 1A (4.0×10^{17} molecules cm^{-3} and 297 K) are representative of

ambient atmosphere conditions. The water concentration in Panel 2A (5.0×10^{17} molecules cm^{-3}) is slightly higher than Panel 1A, but here the spectrum was obtained at an elevated temperature of 312 K. The BBRDS spectrum in Panel 3A was also obtained at 312 K but now with a substantially larger water concentration of 1.4×10^{18} molecules cm^{-3} (which would be above water's saturated vapour pressure at 297 K). Correspondingly, the water monomer structure in Panel 3A is some three times larger than in Panel 2A and almost 4 times larger than Panel 1A, scaling approximately with the water amount. Allowing for the dimer's quadratic dependence on the increased water monomer concentration and for the negative temperature dependence of the equilibrium constant, the water dimer concentration in the sample from Panel 3A is predicted to be a factor of ten larger than in Panel 1A (hence also a factor of ten larger than for typical ambient conditions).

Panels 1B to 3B show the BBRDS residuals from Panels 1A to 3A re-plotted on an expanded vertical scale. Assuming the theoretical line strengths and dimer equilibrium constants from the literature are broadly correct, these panels demonstrate that performing experiments on the high water vapour concentrations available at elevated temperatures in the laboratory ought to produce sufficient water dimer concentrations to yield a measurable dimer signal above the BBRDS baseline noise and/or residuals remaining due to imperfect fitting of the monomer absorbance. The blue Lorentzian function in Panels 1B to 3B represents a generic dimer absorption band of 25 cm^{-1} HWHM. The centre wavelength (748.2 nm) and band strength ($S = 4.5 \times 10^{-22} \text{ cm molecule}^{-1}$) of this dimer feature have been set equal to the average position and average strength of the three theoretical predictions for the $|0\rangle_f |4\rangle_b |0\rangle$ overtone shown in Fig. 2, whilst the dimer concentration giving rise to this absorption was calculated from the square of the water monomer concentration and the temperature dependent equilibrium constant of Curtiss et al. (1979) using Eq. (1b) (any temperature-dependent changes in dimer line strength are likely to be small – see Sect. 5 – and are not considered here). It is evident that, for the conditions of Panel 1B, the measurement residuals are of the same magnitude as the generic dimer feature, and no unequivocal conclusions can be drawn. The generic dimer feature scaled to the conditions of Panel 2B is almost the same size as that in Panel 1B, the slightly greater water monomer concentration being offset by the reduction in K_{eq} at the higher temperature. Once again there is no clear sign of a dimer feature. By comparison, dimer absorption ought to be clearly observable in the BBRDS residual in Panel 3B, where the dimer abundance is expected to be an order of magnitude larger than for the previous panels. Visual inspection indicates little sign of any dimer signal: the peak-to-peak and standard deviation of the residual spectrum in Panel 3B are respectively 5.1×10^{-9} and $1.3 \times 10^{-9} \text{ cm}^{-1}$, i.e. $\times 2.7$ and $\times 11$ smaller than the scaled generic dimer feature for these conditions (peak intensity = $1.4 \times 10^{-8} \text{ cm}^{-1}$).

The immediate conclusion is that either the theoretical predictions significantly over-estimate the dimer line strength, or the variation of K_{eq} with temperature is incorrect. However for the reasons we will set out in the following sections, we prefer an alternative explanation, namely that the dimer absorption band is rather wider than the 25 cm^{-1} HWHM we had assumed here given the previous observational and theoretical work on the dimer (Sect. 1.2).

For comparison, a second feature (dotted red line) in Panels 1B to 3B of Fig. 6 represents the absorption feature described by Pfeilsticker et al. (2003). This feature had a Lorentzian profile centred at 749.5 nm ($13\,342 \text{ cm}^{-1}$) with a FWHM of 19.4 cm^{-1} and a peak absorption of $\alpha = 2.5 \times 10^{-9} \text{ cm}^{-1}$. Like the generic dimer band, the red dotted Lorentzian functions in Panels 1B to 3B have been scaled according to $[\text{H}_2\text{O}]^2$ and the Curtiss et al. (1979) $K_{\text{eq}}(T)$ data to account for differences in water vapour amounts and temperature between the BBRDS measurements and the Pfeilsticker et al. (2003) conditions (292.4 K and $[\text{H}_2\text{O}] = 3.6 \times 10^{17}$ molecules cm^{-3}). Owing to its narrower line width but similar line strength, a dimer absorption band like that originally proposed in Pfeilsticker et al. (2003) would be more readily detectable than the 25 cm^{-1} HWHM dimer bands discussed above, yet no absorption band resembling the red Lorentzian function is observable in any of the BBRDS residuals. Indeed, assignment of the feature reported in Pfeilsticker et al. (2003) to water dimer absorption was subsequently revoked (Lotter, 2006; personal communication from K. Pfeilsticker cited by Garden et al., 2008). In their high resolution cavity ringdown study, Kassi et al. (2005) identified and assigned some 200 additional water monomer lines beyond those included in the HITRAN04 database that had been used to fit the DOAS spectra recorded by Pfeilsticker et al., and suggested that the feature remaining in the DOAS residuals was due at least in part to water lines missing from the reference water cross sections.

Following on from Kassi et al. (2005), an intra-cavity laser absorption spectroscopy (ICLAS) study by Campargue et al. (2008) catalogued 1062 water monomer absorption lines between $12\,746$ and $13\,558 \text{ cm}^{-1}$, a factor of two more lines than produced in the re-analysis of Fourier transform absorption spectra by Tolchenov and Tennyson (2008) which is now adopted in HITRAN08. We noted in the previous section that fitting BBRDS spectra with water monomer cross sections calculated from HITRAN08 produced a broad weak feature in the residual around 745–752 nm (bottom panel of Fig. 5), and this is presumably a result of lines known from the Campargue et al. (2008) study that are yet to be included in HITRAN. As demonstrated again in this section, no such feature is apparent when using the UCL08 line list to fit the BBRDS spectra.

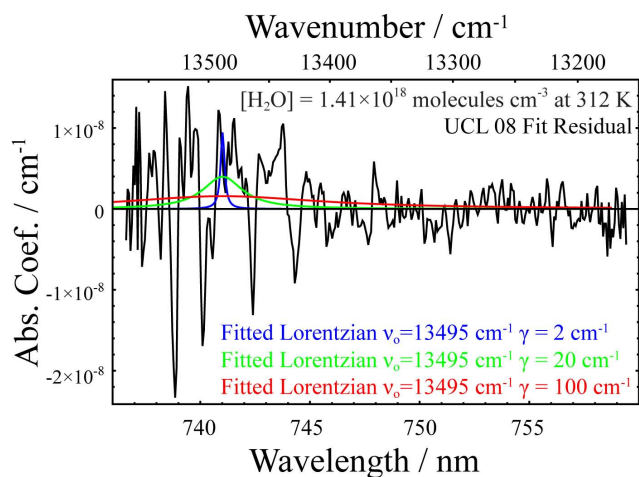


Fig. 7. The BBCRDS residual spectrum from Fig. 6 Panel 3B (black) shown here over the full bandwidth of the BBCRDS measurement. The residual spectrum is fitted with Lorentzian functions of various half widths ($\gamma = 2, 20$ and 100 cm^{-1} ; blue, green and red respectively) centred at the water dimer band frequency predicted by Low and Kjaergaard (1999).

4.3 Characterisation of an upper limit on the water dimer absorption

The fact that no absorption features that can unambiguously be assigned to water dimer absorption have been found in the residuals of BBCRDS spectra reported in this work implies that one or more of the assumptions used to estimate the dimer absorption must be incorrect (the water dimer abundance i.e. $K_{\text{eq}}(T)$; the dimer's calculated line strength; the position and shape of the dimer absorption features). In an attempt to constrain this further, we determine upper limits for water dimer absorption in the 736–759 nm spectral region by considering what signal, if any, remains in the BBCRDS measurements that cannot be attributed to water monomer absorption using the UCL08 database. The BBCRDS measurement at $[\text{H}_2\text{O}] = 1.41 \times 10^{18} \text{ molecules cm}^{-3}$ and 312 K was selected for this analysis (Panel 3A/B of Fig. 6), since these conditions are expected to produce the greatest dimer absorption signal. The fitted BBCRDS spectrum's residual, shown again on an expanded scale in Fig. 7, contains some systematic structure much of which is undoubtedly the result of still imperfect treatment of the water monomer absorption but which, nevertheless, could overlie a weak dimer signal.

To derive upper limits for possible water dimer absorption, the approach taken was to fit Lorentzian functions with variable widths, representative of water dimer absorption features of differing widths, to the BBCRDS residual. Fig. 7 shows fitted Lorentzian features constrained to be centred at 13495 cm^{-1} (741.0 nm), i.e. at the Hartree–Fock prediction of Low and Kjaergaard (1999), with example HWHMs of $\gamma = 2, 20$ and 100 cm^{-1} . ($\gamma = 2 \text{ cm}^{-1}$ corresponds to the

narrowest feature resolvable with present BBCRDS instrument's function of 0.22 nm FWHM at 750 nm). There happens to be a positive feature in the BBCRDS residual spectrum at 13495 cm^{-1} which, for the narrowest dimer line width considered here, leads the Lorentzian line fitting routine to produce a putative dimer absorption signal peaking around $1 \times 10^{-8} \text{ cm}^{-1}$. However, the peak of this fitted Lorentzian quickly reduces as the line width broadens to more realistic values for a dimer absorption band as more negative (and only weakly positive) residual structure becomes incorporated into the fit.

The black dots shown in Panel A of Fig. 8 represent the peak intensity of the Lorentzian function (centred at 13495 cm^{-1}) that can be fitted to the BBCRDS residual spectrum plotted against the Lorentzian's HWHM. The pink region shows the 1σ uncertainty in the fitted Lorentzian's intensity. The various lines in the blue region (same line types as the legend to Fig. 1) show the expected peak absorption for a Lorentzian shaped dimer feature calculated as a function of half width (γ) for different literature values of K_{eq} :

$$\text{Peak absorption} = \frac{S \times [\text{H}_2\text{O}]^2 \times K_{\text{eq}}}{\pi \times \gamma} \quad (3)$$

where, for Panel A, the dimer line strength was assumed to be the Hartree–Fock value of $S = 4.83 \times 10^{-22} \text{ cm molecule}^{-1}$ from Low and Kjaergaard (1999). The lower and upper boundaries of the blue region thus correspond to the minimum and maximum K_{eq} estimates of Munoz-Caro and Nino (1997) and Goldman et al. (2004) respectively.

Taking the K_{eq} estimate of Curtiss et al. (1979) as (i) intermediate and hence representative of all the available K_{eq} values, and (ii) a K_{eq} determined from experiment, the plot in the top panel of Fig. 8 indicates that the HWHM of any water dimer feature must be rather larger than 100 cm^{-1} because at no point on the graph does the upper limit for dimer absorption from fitting the BBCRDS residual (top of pink region) coincide with the theoretical prediction of the water dimer absorption (Curtiss K_{eq} = thick black dashed line in the blue region). If however one assumes that the lowest K_{eq} estimate of Munoz-Caro and Nino (1997) is correct, then the measurements imply a minimum HWHM consistent with the upper limit on our experimental uncertainty of approximately 20 cm^{-1} , or more likely 30 cm^{-1} HWHM for the optimum Lorentzian fit (black points). Thus the analysis here leads to a HWHM-dependent upper limit for the water dimer absorption signal, dependent also on which K_{eq} is adopted. It should be noted that the discussion assumes that the chosen theoretical prediction of the water dimer line parameters is correct. (Low and Kjaergaard (1999) produced another prediction of this dimer band's position and line strength using a quadratic configuration interaction level of theory: 13403 cm^{-1} (746.1 nm) and $3.04 \times 10^{-22} \text{ cm molecule}^{-1}$. These values happen to be close to those considered in the next paragraph, and we would expect the same conclusions to apply).

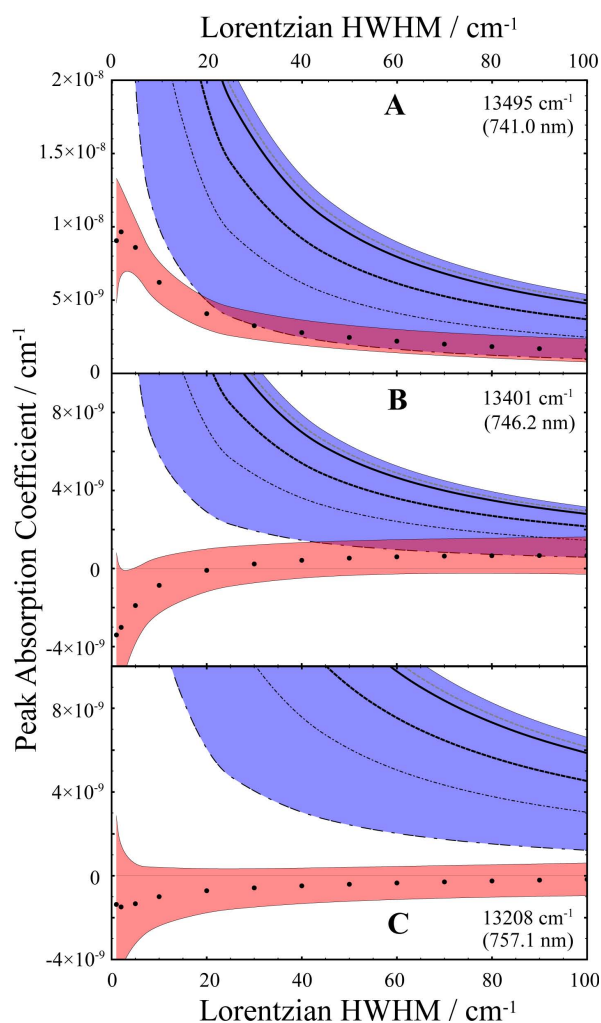


Fig. 8. Upper limits on any dimer signal remaining in the BCCRDS residual spectrum. Panel A: The peak intensity (black dots) of Lorentzian functions fitted to the BCCRDS residual spectrum shown previously in Fig. 7. The Lorentzian function is centred at 741.0 nm (Low and Kjaergaard, 1999) and has a variable HWHM of $\gamma = 1, 2, 5, 10, 20, \dots, 100 \text{ cm}^{-1}$. The pink shaded area represents the 1σ uncertainty in the fitted Lorentzian function's peak intensity. The various solid and dashed lines in the blue envelope are HWHM-dependent absorption coefficients for the dimer calculated via Eq. (3) using the various values of K_{eq} from the literature (same line types as Fig. 1) and the Hartree-Fock dimer line strength of Low and Kjaergaard (1999): see the main text. Panels B and C are analogous plots generated by fitting the BCCRDS residual spectrum with Lorentzian functions centred at 746.2 nm (Schofield and Kjaergaard, 2003) and 757.1 nm (Schofield et al., 2007).

Panel B of Fig. 8 has the same format as Panel A except that the central wavelength of the fitted Lorentzian function and the water dimer line strength are now constrained at 13401 cm^{-1} (746.2 nm) and $2.83 \times 10^{-22} \text{ cm molecule}^{-1}$ (Schofield and Kjaergaard, 2003). For this case, the peak absorption is negative for narrow Lorentzian features due to

negative structure (measurement noise and/or imperfectly fitted water monomer absorption) being present in the residual spectrum at this centre wavelength. Again, the main conclusion is that if the K_{eq} values of Curtiss et al. (1979) and Munoz-Caro and Nino (1997) are adopted, the minimum HWHM for dimer transitions must be greater than 100 cm^{-1} or around 40 cm^{-1} respectively to be consistent with the upper uncertainty limit in any dimer-like Lorentzian feature present in the BCCRDS residual spectrum (top of the pink shaded region) or rather more than 100 cm^{-1} or around 80 cm^{-1} respectively for the optimum fitted Lorentzian functions (black dots). Panel C of Fig. 8 assumes the Lorentzian dimer feature lies at 13208 cm^{-1} (757.1 nm) with a line strength of $5.93 \times 10^{-22} \text{ cm molecule}^{-1}$ according to the AVQZ numeric potential energy curve calculation preferred by Schofield et al. (2007). At this wavelength, the inferred minimum HWHM of dimer transitions is greater than 100 cm^{-1} irrespective of the choice of K_{eq} .

Similar conclusions are drawn when the wavelength restriction is lifted and Lorentzian functions of variable HWHM are now fitted sequentially at centres every 2 cm^{-1} between 13586 and 13166 cm^{-1} across the BCCRDS measurement's bandwidth. Here the dimer line strength was taken to be the most restrictive of those from the theoretical calculations ($S = 2.83 \times 10^{-22} \text{ cm molecule}^{-1}$, Schofield and Kjaergaard, 2003). The black dots in the upper panel of Fig. 9 now show the mean peak intensity of the many Lorentzian functions fitted over this frequency range, and the pink region denotes one standard deviation about their mean intensity. Again, the minimum HWHM of the dimer absorption must be greater than 100 cm^{-1} to be consistent with the preferred Curtiss et al. (1979) value of K_{eq} . Using the greater line strengths from Low and Kjaergaard (1999) or Schofield et al. (2007) increases the predicted dimer peak absorption even further above the maximum signal remaining in the BCCRDS residual spectrum, again confirming that any dimer feature residing in the BCCRDS residual must be very wide indeed to be consistent with the theoretical studies.

Equivalently, via a rearrangement of Eq. (3), one can assume that a particular K_{eq} is correct, and then infer the line strength of a dimer transition that would be necessary to reproduce the maximum Lorentzian function consistent with the BCCRDS residual – see the lower panel of Fig. 9. The analogous result is obtained: only the smallest K_{eq} values are consistent with the Lorentzian dimer absorptions fitted to the BCCRDS residual spectrum, and only then for HWHM values greater than at least 80 cm^{-1} assuming the weakest of the line strengths predicted by theory (horizontal red line; Schofield and Kjaergaard, 2003). The dimer's Lorentzian half width has to be substantially greater than 100 cm^{-1} for the upper limit of any signal in the BCCRDS residual to be consistent with the line strengths predicted by Low and Kjaergaard (1999) or Schofield et al. (2007) (blue or black lines), particularly if the Curtiss et al. (1979) equilibrium constant is adopted.

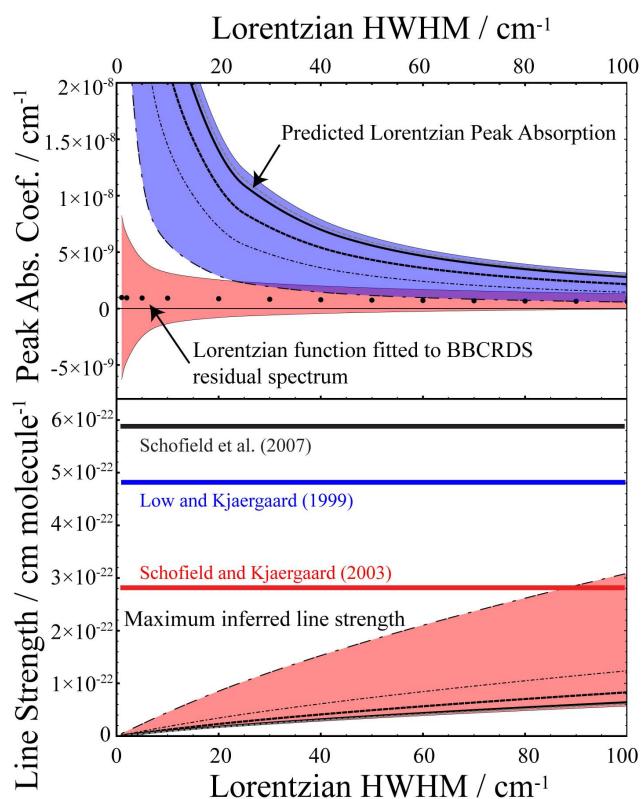


Fig. 9. Upper panel: an analogous plot to Fig. 8 for the average intensity of Lorentzian functions fitted to the BBRDS residual spectrum in 2 cm⁻¹ intervals across the full measurement bandwidth. The predicted peak absorption (blue envelope enclosing the various $K_{\text{eq}}(T)$ values) was calculated using the smallest dimer band intensity from theory: $S = 2.83 \times 10^{-22}$ cm molecule⁻¹ (Schofield and Kjaergaard, 2003). Lower panel: upper limits on the dimer line strengths consistent with the BBRDS residuals calculated as a function of Lorentzian HWHM (using black dots data from the upper panel) for the different literature values of K_{eq} (lines in pink regions). Line strengths from the theoretical studies are shown as the heavy horizontal lines.

5 Discussion of results

From the water dimer perspective, the main conclusion of this study is that the line shape of any water dimer absorption in the 750 nm region must be rather wider than the 25–30 cm⁻¹ HWHM previously observed for smaller excitations at frequencies further into the infrared (Ptashnik et al., 2004, 2011; Paynter et al., 2007; Ptashnik, 2008). The minimum HWHM for dimer transitions inferred here depends on both the value of K_{eq} and the dimer line strength calculated by theory, and hence an error in either (or both) of these quantities would impact our conclusion. If the smallest K_{eq} values are used, then relatively narrow (25 cm⁻¹ HWHM) water dimer features could be consistent with the residuals in our BBRDS observations; although this also supposes the dimer band occurs closest to the water monomer band where

the structure remaining in the BBRDS residual is greatest (Fig. 8 Panel A). But it has become generally accepted (Ptashnik, 2008) that K_{eq} is uncertain by no more than approximately $\pm 25\%$ about the Curtiss et al. (1979) data, and thus the upper limits placed on the dimer absorption from this work are more probably only consistent with a very broad dimer absorption (HWHM > 100 cm⁻¹). This discussion assumes that the dimer line strength calculated by theory is broadly correct, and indeed the line strengths are generally thought to be uncertain by only a factor of two. For example, the range of intensities predicted by the many different levels of theory considered by Schofield et al. (2007) spanned a factor of two. A similar conclusion can be drawn from the intensities of the various calculated dimer spectra shown in the bottom panel of Fig. 2 which were deliberately chosen to span the full range of band positions and band intensities represented in recent literature. Kjaergaard et al. (2008) also showed that different vibrational models still produced similar calculated overtone intensities (albeit only trialed up to the $\nu = 2$ OH stretch), further supporting the range of intensity values adopted in our study. Temperature effects, other than for the monomer concentration and equilibrium constant which are already considered, are not expected to change our main conclusion because variation in the dimer line strength with temperature is thought to be small (around 10% over the temperature range of this study) (Paynter, 2008).

After the reported water dimer detection by Pfeilsticker et al. (2003), Suhm (2004) commented that one would expect the overtone transitions of a relatively weakly bound species such as the water dimer to be considerably broader (by up to an order of magnitude) than the 9.7 cm⁻¹ HWHM inferred by Pfeilsticker et al. because, at ambient temperature, the lifetime of an individual dimer is sufficiently short that a range of hydrogen bond strengths are likely within a collection of dimer molecules. A further effect and one that until recently was not included in theoretical calculations is coupling of the OH_b stretch with other intra-molecular oscillations which can lead to a considerable broadening of spectral structure. The theoretical study of Garden et al. (2008) attempted to include coupling effects when calculating the band profiles for water dimer transitions. Although Garden et al. (2008) still only considered transitions between a restricted set of dimer vibrational states, their calculations did address the most important O–O stretching motion, excitation of which has the greatest effect in modifying the potential energy curve for the hydrogen-bonded OH stretch. Garden et al.'s (2008) results suggest that, whilst each transition may only be around 20 cm⁻¹ HWHM, the summation of many vibrational bands is likely to produce a much broader feature (in the limit, something more like a continuum), with the intensity of a given OH_b stretching overtone now shared between many simultaneously excited O–O stretches. Garden et al. (2008) also found that the effective widths of dimer transitions increased with increasing overtone. (Similarly, Howard and Kjaergaard (2006) observed the intra-molecular

hydrogen-bonded OH stretch in 1,3-propanediol and 1,4-butanediol to become broad for high overtones: HWHM $\approx 360 \text{ cm}^{-1}$ for $\nu = 4$). In the 750 nm region investigated in the present work, the superposition of multiple OH_b water dimer transitions simultaneously promoting different excitations elsewhere in the dimer molecule was calculated by Garden et al. (2008) to be very broad, covering several hundred cm^{-1} (so HWHM of the order of at least 100 cm^{-1}), and as such is entirely consistent with our own conclusion.

Our results may also explain why previous attempts to search for signs of water dimer absorption in the atmosphere itself have been unsuccessful or inconclusive (e.g. Daniel et al., 1999; Hill and Jones, 2000; Sierk et al., 2004). It was not because the calculated dimer line strength was incorrect, as was supposed at the time, but because the width of the transitions are probably so large that any dimer signals that may have been present in the measured spectra would easily have been lost in the experimental noise and/or removed as the fitted broadband continuum in any DOAS analysis.

6 Conclusions

The intention of this work was to search for signs of water dimer absorption at wavelengths around 750 nm where theoretical studies predict the $|0\rangle_f |4\rangle_b |0\rangle$ OH_b stretching overtone to occur. Allied to this effort, a new database of water monomer absorption lines was constructed from the best experimental and theoretical data currently available. This UCL08 line list covers the frequency range 750–20 000 cm^{-1} and is presented in HITRAN file format in this paper's accompanying data. The intensity-weighted average line strengths in UCL08 are within 2.5 % of HITRAN08 in most spectral regions (although there are larger line-by-line differences, especially for weaker lines), but is some 20 % stronger for UCL08 in the 8000–9500 cm^{-1} region. Of direct relevance to our search for a water dimer signal, the UCL08 list contains many additional lines in “quieter” spectral regions in between monomer bands, i.e. in regions offering experimental advantages for observing red-shifted dimer bands. It may also be worth incorporating the extra monomer lines in radiative budget calculations, (c.f. Learner et al., 1999; Zhong et al., 2001). Compared to HITRAN08, the UCL08 line list was found to produce a better fit to the monomer structure (smaller residuals) in broadband cavity ringdown spectra of water vapour in the wavelength region 736–759 nm.

Laboratory measurements made to attempt to reproduce the absorption feature observed by Pfeilsticker et al. (2003) found no such signal in the BBRDS spectra. Experiments conducted at high relative humidity and elevated temperatures (up to 85 % RH at 312 K) to increase the dimer number concentration by a factor of ten above ambient conditions also found no signal that could unambiguously be assigned to water dimer absorption when the new UCL08 database

was used to fit the water monomer component of BBRDS spectra. Moreover, if the dimer signal is constrained to have a half width similar to that observed for the dimer's fundamental, first overtone and low combination bands (HWHM $\approx 25 \text{ cm}^{-1}$), water dimer absorptions calculated using dimer line intensities available from theoretical studies and the Curtiss et al. (1979) equilibrium constant were found to be much greater than the maximum possible dimer signal in the BBRDS spectra. The Curtiss et al. (1979) K_{eq} values are thought to be broadly correct and since it is unlikely that water dimer line strengths from theory could be wrong by an order of magnitude, this result implies that the HWHM of the high overtone water dimer absorptions must be somewhat greater than previously observed for the lower energy dimer bands further into the infrared. The HWHM inferred for water dimer transitions in the present 750 nm region ($\geq 100 \text{ cm}^{-1}$) is consistent with predictions from recent theoretical work that show OH_b dimer bands becoming increasingly broad for higher vibrational overtones due to coupling of the stretching motion with other internal modes of the molecule (Garden et al., 2008). The width of dimer absorption bands (e.g. how far they extend into regions between the water monomer bands) determines the amount of solar radiation absorbed by the dimer, and hence the dimer's feedback role in climate change. The BBRDS measurements described here provide a useful observational limit to aid further calculations to predict the shape and magnitude of water dimer absorption.

Supplement related to this article is available online at:
<http://www.atmos-chem-phys.net/11/4273/2011/acp-11-4273-2011-supplement.pdf>.

Acknowledgements. This work was conducted within the CAVIAR consortium supported by the Natural Environment Research Council. We specifically acknowledge PhD studentships for A.J.L.S. and M.J.B., and grant awards to Cambridge University (NE/D013046/1), Leicester University (NE/D010853/1) and University College London (NE/D013003/1). We thank R. J. Barber for his assistance with including theoretical lines in the UCL08 list, and colleagues within the CAVIAR consortium (notably Igor Ptashnik) for many informative discussions on water vapour's spectroscopy. We acknowledge our discussion paper's two referees whose comments helped improve the final manuscript.

Edited by: J. B. Burkholder

References

- Aldener, M., Brown, S. S., Stark, H., Daniel, J. S., and Ravishankara, A. R.: Near-IR absorption of water vapour: pressure dependence of line strengths and an upper limit for continuum absorption, *J. Molec. Spectrosc.*, 232, 223–230, 2005.
- Ball, S. M. and Jones, R. L.: Broad-band cavity ring-down spectroscopy, *Chem. Rev.*, 103, 5239–5262, doi:10.1021/cr020523k, 2003.
- Ball, S. M. and Jones, R. L.: Broadband cavity ring-down spectroscopy in “Cavity ring-down spectroscopy: techniques and applications”, edited by: Berden, G. and Engeln, Blackwell Publishing Ltd, Chichester, West Sussex, UK, 57–88, 2009.
- Barber, R. J., Tennyson, J., Harris, G. J., and Tolchenov, R. N.: A high-accuracy computed water line list, *Mon. Not. R. Astron. Soc.*, 368, 1087–1094, 2006.
- Bitter, M., Ball, S. M., Povey, I. M., and Jones, R. L.: A broad-band cavity ringdown spectrometer for in-situ measurements of atmospheric trace gases, *Atmos. Chem. Phys.*, 5, 2547–2560, doi:10.5194/acp-5-2547-2005, 2005.
- Bouteiller, Y. and Perchard, J. P.: The vibrational spectrum of (H₂O)₂: comparison between anharmonic ab initio calculations and neon matrix infrared data between 9000 and 90 cm⁻¹, *Chem. Phys.*, 305, 1–12, 2004.
- Campargue, A., Mikhailenko, S., and Liu, A. W.: ICLAS of water in the 770 nm transparency window (12,746 – 13,558 cm⁻¹). Comparison with current experimental and calculated databases, *J. Quant. Spectrosc. Radiat. Transf.*, 109, 2832–2845, 2008.
- Casanova, S. E. B., Shine, K. P., Gardiner, T., Coleman, M. and Pegrum, H.: Assessment of the consistency of near-infrared water vapor line intensities using high-spectral-resolution ground-based Fourier transform measurements of solar radiation, *J. Geophys. Res. Atmos.*, 111, D11302, doi:10.1029/2005JD006583, 2006.
- Cormier, J. G., Hodges, J. T., and Drummond, J. R.: Infrared water vapour continuum absorption at atmospheric temperatures, *J. Chem. Phys.*, 122, 114309, doi:10.1063/1.1862623, 2005.
- Coudert, L. H., Wagner, G., Birk, M., Baranov, Yu. I., Lafferty, W. J., and Flaud, J.-M.: The H₂¹⁶O molecule: Line position and line intensity analyses up to the second triad, *J. Mol. Spectrosc.*, 251, 339–357, 2008.
- Curtiss, L. A., Frurip, D. J., and Blander, M.: Studies of molecular association in H₂O and D₂O vapors by measurement of thermal conductivity, *J. Chem. Phys.*, 71, 2703–2711, 1979.
- Chýlek, P. and Geldart, D. J. W.: Water vapor dimers and atmospheric absorption of electromagnetic radiation, *Geophys. Res. Lett.*, 24(16), 2015–2018, 1997.
- Daniel, J. S., Solomon, S., Sanders, R. W., Portmann, R. W., Miller, D. C., and Madsen, W.: Implications for water monomer and dimer solar absorption from observations at Boulder, Colorado, *J. Geophys. Res. Atmos.*, 104, 16785–16791, 1999.
- Fellers, R. S., Leforestier, C., Braly, L. B., Brown, M. G., and Saykally, R. J.: Spectroscopic determination of the water pair potential, *Science*, 284, 945–948, 1999.
- Garden, A. L., Halonen, L., and Kjaergaard, H. G.: Calculated band profiles of the OH-stretching transitions in water dimer, *J. Phys. Chem. A*, 112, 7439–7447, doi:10.1021/jp802001g, 2008.
- Goldman, N., Leforestier, C., and Saykally, R. J.: Water dimers in the atmosphere II: Results from the VRT(ASP-W)III potential surface, *J. Phys. Chem. A*, 108, 787–794, doi:10.1021/jp035360y, 2004.
- Harvey, A. H. and Lemmon, E. W.: Correlation for the second virial coefficient of water, *J. Phys. Chem. Ref. Data*, 33, 369–376, doi:10.1063/1.1587731, 2004.
- Hill, C. and Jones, R. L.: Absorption of solar radiation by water vapor in clear and cloudy skies: Implications for anomalous absorption, *J. Geophys. Res. (Atmos.)*, 105, 9421–9428, 2000.
- Howard, D. L. and Kjaergaard, H. G.: Influence of intramolecular hydrogen bond strength on OH-stretching overtones, *J. Phys. Chem. A*, 110, 10245–10250, doi:10.1021/jp063631, 2006.
- Huisken, F., Kaloudis, M., and Kulcke, A.: Infrared spectroscopy of small size-selected water clusters, *J. Chem. Phys.* 104, 17–25, 1996.
- Ishuchi, S., Fujii, M., Robinson, T. W., Miller, B. J., and Kjaergaard, H. G.: Vibrational overtone spectroscopy of phenol and its deuterated isotopomers, *J. Phys. Chem. A*, 110, 7345–7354, doi:10.1021/jp060723q, 2006.
- Jenouvrier, A., Daumont, L., Regalia-Jarlot, L., Tyuterev, V. G., Carleer, M., Vandaele, A. C., Mikhailenko, S., and Fally, S.: Fourier transform measurements of water vapor line parameters in the 4200–6600 cm⁻¹ region, *J. Quant. Spectrosc. Radiat. Transf.*, 105, 326–355, 2007.
- Kassi, S., Macko, P., Naumenko, O., and Campargue, A.: The absorption spectrum of water near 750 nm by CW-CRDS: contribution to the search of water dimer absorption, *Phys. Chem. Chem. Phys.*, 7, 2460–2467, 2005.
- Kjaergaard, H. G., Garden, A. L., Chaban, G. M., Gerber, R. B., Matthews, D. A., and Stanton, J. F.: Calculation of vibrational transition frequencies and intensities in water dimer: comparison of different vibrational approaches, *J. Phys. Chem. A*, 112, 4324–4335, doi:10.1021/jp710066f, 2008.
- Kuyanov-Prozument, K., Choi, M. Y., and Vilesov, A. F.: Spectrum and infrared intensities of OH-stretching bands of water dimers, *J. Chem. Phys.*, 132, 014304, doi:10.1063/1.3276459, 2010.
- Learner, R. C. M., Zhong, W., Haigh, J. D., Belmiloud, D., and Clarke, J.: The contribution of unknown weak water vapor lines to the absorption of solar radiation, *Geophys. Res. Lett.*, 26, 3609–3612, 1999.
- Lotter, A.: Field measurements of water continuum and water dimer absorption by active long path differential optical absorption spectroscopy (DOAS), PhD thesis, Department of Physics, University of Heidelberg, Germany, 2006.
- Low, G. R., and Kjaergaard, H. G.: Calculation of OH-stretching band intensities of the water dimer and trimer, *J. Chem. Phys.*, 110, 9104–9115, 1999.
- Mikhailenko, S. N., Le, W., Kassi, S., and Campargue, A.: Weak water absorption lines around 1.455 and 1.66 μm by CW-CRDS, *J. Mol. Spectrosc.*, 244/2, 170–178, 2007.
- Mikhailenko, S. N., Albert, K. A. K., Mellau, G., Klee, S., Winnewisser, B. P., Winnewisser, M., and Tyuterev, V. G.: Water vapor absorption line intensities in the 1900–6600 cm⁻¹ region, *J. Quant. Spectrosc. Radiat. Transf.*, 109, 2687–2696, 2008.
- Munoz-Caro, C., and Nino, A.: Effect of anharmonicities on the thermodynamic properties of the water dimer, *J. Phys. Chem. A*, 101, 4128–4135, 1997.
- Nizkorodov, S. A., Ziemkiewicz, M., Nesbitt, D. J., and Knight, A. E. W.: Overtone spectroscopy of H₂O clusters in the ν_{OH} = 2 manifold: infrared-ultraviolet vibrationally mediated dissociation studies, *J. Chem. Phys.*, 122, 194316, doi:10.1021/jp035360y, 2004.

- doi:10.1063/1.1899157, 2005.
- Odutola, J. A. and Dyke, T. R.: Partially deuterated water dimers – microwave spectra and structure, *J. Chem. Phys.*, 72, 5062–5070, 1980.
- Paul, J. B., Collier, C. P., Saykally, R. J., Scherer, J. J., and O’Keefe, A.: Direct measurement of water cluster concentrations by infrared cavity ringdown laser absorption spectroscopy, *J. Phys. Chem. A*, 101, 5211–5214, 1997.
- Paul, J. B., Provencal, R. A., and Saykally, R. J.: Characterisation of the (D₂O)₂ hydrogen-bond-acceptor antisymmetric stretch by IR cavity ringdown laser absorption spectroscopy, *J. Phys. Chem. A*, 102, 3279–3283, 1998.
- Paynter, D. J.: Measurements and interpretations of the water vapour continuum at near infrared wavelengths, PhD thesis, Department of Meteorology, University of Reading, UK, 2008.
- Paynter, D. J., Ptashnik, I. V., Shine, K. P., and Smith, K. M.: Pure water vapor continuum measurements between 3100 and 4400 cm⁻¹: Evidence for water dimer absorption in near atmospheric conditions, *Geophys. Res. Lett.*, 34(12), L12808, doi:10.1029/2007GL029259, 2007.
- Paynter, D. J., Ptashnik, I. V., Shine, K. P., Smith, K. M., McPheat, R., and Williams, R. G.: Laboratory measurements of the water vapor continuum in the 1200–8000 cm⁻¹ region between 293 K and 351 K, *J. Geophys. Res. (Atmos.)*, 114, D21301, doi:10.1029/2008JD011355, 2009.
- Pfeilsticker, K., Lotter, A., Peters, C., and Bösch, H.: Atmospheric detection of water dimers via near-infrared absorption, *Science*, 300, 2078–2080, 2003.
- Platt, U.: Modern methods of the measurement of atmospheric trace gases, *Phys. Chem. Chem. Phys.*, 1, 5409–5415, 1999.
- Ptashnik, I. V.: Evidence for the contribution of water dimers to the near-IR water vapour self-continuum, *J. Quant. Spectrosc. Radiat. Transf.*, 109, 831–852, 2008.
- Ptashnik, I. V., Smith, K. M., Shine, K. P., and Newnham, D. A.: Laboratory measurements of water vapour continuum absorption in spectral region 5000–5600 cm⁻¹: Evidence for water dimers, *Q. J. Roy. Meteorol. Soc.*, 130, 2391–2408, doi:10.1256/qj.03.178, 2004.
- Ptashnik, I. V., Shine, K. P., and Vigasin, A. A.: Water vapour self-continuum and water dimers: 1. Analysis of recent work, *J. Quant. Spectrosc. Radiat. Transf.*, doi:10.1016/j.jqsrt.2011.01.012, in press, 2011.
- Rothman, L. S., Gordon, I. E., Barbe, A., Benner, D. C., Bernath, P. E., Birk, M., Boudon, V., Brown, L. R., Campargue, A., Champion, J. P., Chance, K., Coudert, L. H., Dana, V., Devi, V. M., Fally, S., Flaud, J. M., Gamache, R. R., Goldman, A., Jacquemart, D., Kleiner, I., Lacome, N., Lafferty, W. J., Mandin, J. Y., Massie, S. T., Mikhailenko, S. N., Miller, C. E., Moazzen-Ahmadi, N., Naumenko, O. V., Nikitin, A. V., Orphal, J., Perevalov, V. I., Perrin, A., Predoi-Cross, A., Rinsland, C. P., Rotger, M., Simeckova, M., Smith, M. A. H., Sung, K., Tashkun, S. A., Tennyson, J., Toth, R. A., Vandaele, A. C., and Vander Auwera, J.: The HITRAN 2008 molecular spectroscopic database, *J. Quant. Spectrosc. Radiat. Transf.*, 110, 533–572, doi:10.1016/j.jqsrt.2009.02.013, 2009.
- Schofield, D. P. and Kjaergaard, H. G.: Calculated OH-stretching and HOH-bending vibrational transitions in the water dimer, *Phys. Chem. Chem. Phys.*, 5, 3100–3105, doi:10.1039/b304952c, 2003.
- Schofield, D. P., Lane, J. R., and Kjaergaard, H. G.: Hydrogen bonded OH-stretching vibration in the water dimer, *J. Phys. Chem. A*, 111, 567–572, doi:10.1021/jp063512u, 2007.
- Scribano, Y., Goldman, N., Saykally, R. J., and Leforestier, C.: Water dimers in the atmosphere III: Equilibrium constant from a flexible potential, *J. Phys. Chem. A*, 110, 5411–5419, doi:10.1021/jp056759k, 2006.
- Sierk, B., Solomon, S., Daniel, J. S., Portmann, R. W., Gutman, S. I., Langford, A. O., Eubank, C. S., Dutton, E. G., and Holub, K. H.: Field measurements of water vapour continuum absorption in the visible and near-infrared, *J. Geophys. Res. Atmos.*, 109, D08307, doi:10.1029/2003JD003586, 2004.
- Suhm, M. A.: How broad are water dimer bands?, *Science*, 304, 823–823, 2004.
- Tennyson, J., Zobov, N. F., Williamson, R., Polyansky O. L., and Bernath, P. F.: Experimental energy levels of the water molecule, *J. Phys. Chem. Ref. Data*, 30, 735–831, 2001.
- Tolchenov, R. and Tennyson J.: Water line parameters from refitted spectra constrained by empirical upper state levels: study of the 9500–14500 cm⁻¹ region, *Quant. Spectrosc. Radiat. Transf.*, 109, 559–568, 2008.
- Vigasin, A. A.: Water vapor continuous absorption in various mixtures: possible role of weakly bound complexes, *J. Quant. Spectrosc. Radiat. Transf.*, 64, 25–40, 2000.
- Voronin, B. A., Lavrentieva, N. N., Mishina, T. P., Chesnokova, T. Yu., Barber, M. J., and Tennyson, J.: Estimate of the J’ J’’ dependence of water vapor line broadening parameters, *J. Quant. Spectrosc. Radiat. Transf.*, 111, 2308–2314, doi:10.1016/j.jqsrt.2010.05.015, 2010.
- Zhong, W., Haigh, J. D., Belmiloud, D., Schermaul R., and Tennyson, J.: The impact of new water vapour spectral line parameters on the calculation of atmospheric absorption, *Q. J. Roy. Meteorol. Soc.*, 127, 1615–1626, 2001.